

Non-magnetic impurity doping effect on the magnetic state of p-type Al-doped delafossite oxide CuCrO_2

Research Article

Fatma Jlaiei¹, Mongi Amami^{1,2*}, Piere Strobel²,
Abdelhamid Ben Salah¹

¹Laboratory of Materials Science and Environment,
University of Sfax, 3038 Sfax, Tunisia

²Joseph Fourier Néel Institute - CNRS,
38042 Grenoble Cedex 9, France

Received 3 January 2011; Accepted 16 May 2011

Abstract: We investigated the substitution effects of Al^{3+} for Cr^{3+} on the structure and magnetic, properties of delafossite oxide CuCrO_2 , which possesses a quasi-2D Heisenberg triangular antiferromagnetic (AFM) lattice. The lattice parameters was found to vary according to the Vegard's rule. We also found that the large local lattice distortion, caused by the nonmagnetic dopant with different radii between magnetic and nonmagnetic ions, affects the samples significantly.

Magnetization and specific heat measurements indicated that AFM ordering is diluted by the substitution of nonmagnetic Al^{3+} for Cr^{3+} ($S = 3/2$).

Keywords: Delafossite • Microstrain • Magnetism • Specific heat

© Versita Sp. z o.o.

1. Introduction

AMO_2 delafossite compounds derived from the CuFeO_2 mineral are quite interesting materials because of their ability to be stabilized with a large number of A and M cations and within a wide range of off-stoichiometry values, which leads to different physical properties [1,2]. In particular, delafossite compounds with $M = \{\text{Al}, \text{Ga}\}$ have attracted much attention as p-type transparent conducting oxides (TCOs) in the past decade [3]. Nowadays, studies on delafossite oxides are interesting not only for the TCO properties but also for the applications such as in catalysis [4], magnetics [5], and possibly thermoelectric [6,7].

The delafossite structure can accommodate monovalent noble metal cations $A^+ = \{\text{Cu}^+, \text{Ag}^+, \text{Pd}^+, \text{Pt}^+\}$ and trivalent cations M^{3+} with ionic radii varying from 0.535 Å (octahedral Al^{3+} ion) up to 1.032 Å (octahedral La^{3+} ion) according to Shannon's table of effective ionic radii [8]. The AMO_2 delafossite structure can be described as a stacking of MO_2 layers made of edge-sharing MO_6 octahedra that are connected by planes of A^+ cations

arranged as a triangular network. Each A^+ cation is linearly coordinated by two O- anions belonging to the upper and lower MO_2 layers. The oxygen layers can be stacked in different ways along the c axis in order to form two polytypes of the delafossite structure: the hexagonal 2H (space group P63/mmc) and the rhombohedral 3R (space group R3m) polytypes.

Recently the chemical impurity effect on the magnetic properties of CuFeO_2 has been studied [9–16]. In particular, nonmagnetic impurity strongly affects the magnetic properties of $\text{CuFe}_{1-x}\text{Al}_x\text{O}_2$ by disturbing the delicate balance of the competing exchange interactions. As a result, the quasi-Ising character of CuFeO_2 disappears due to the substitution of a small amount of non-magnetic impurity.

Here we focus on the effect of nonmagnetic Al^{3+} impurity on the magnetic, transport, and specific heat properties of CuCrO_2 ($\text{CuCr}_{1-x}\text{Al}_x\text{O}_2$). The later composition was theoretically studied for some fixed composition (almostly $x = 0.5$) [17], and the synthesis of the sample has just been addressed by one recent publication [18].

* E-mail: mongi.amami@ipein.rnu.tn

2. Experimental procedure

Polycrystalline samples of CuCr_{1-x}Al_xO₂ were prepared with *x* from 0.0 up to 0.40 by step of 0.05. Stoichiometric mixtures (0.5 g) of Cu₂O, Cr₂O₃ and Al₂O₃ were ground and pressed in pellets. Samples were fired in air at 1050°C for 12 h in high-purity alumina crucibles. The obtained mixture was ground and calcined several times in air at 1100°C with a grinding procedure repeated at regular intervals.

X-ray powder diffraction patterns of the reacted pellets were collected with a PANalytical diffractometer equipped with a CuKα source (Kα1 and Kα2) in the 2θ range from 10° to 90° at room temperature. Strain and size components were extracted from line widths using the Williamson-Hall (WH) analysis [10]. This method uses the fact that the crystallite size contribution varies as tan θ. The equation used is

$$L \cdot \cos \theta = \frac{\lambda}{D} + k\epsilon \sin \theta$$

Where *L* is the integral width, λ is the wavelength used, *D* is the size of the coherent diffraction domain, *k* is a near-unity constant, and ϵ is the microstrain term. The plot of (*L*·cosθ) as a function of (sinθ) yields *D* from the intercept and ϵ from the slope.

The dependence of magnetization on applied field and temperature was measured in a Quantum Design superconducting quantum interference device (SQUID) magnetometer in the temperature range 2.0-300 K. The typical field used for temperature dependence measurements was 0.1 T. Specific heat was measured in zero magnetic field by a relaxation method.

3. Result and discussion

3.1. Structural characterizations

The investigated samples are isostructural with the delafossite 3R polytype (space group R-3m) and no additional peak such as superstructure reflection was found at any *x*-value.

00*l* peaks are sharp, but other (*h*0*l*) peaks are broadened, shifted and asymmetric due to stacking faults perpendicular to the *c* axis (Fig. 1). Above 0.4 the broadening of the peak is very important in a way that the phase identification is risky. Considering the differences in the radii of Cr³⁺ (0.063 nm) and Al³⁺ (0.051 nm), the possibility of substituting one metal ion by the other in the full range 0 < *x* < 1 is surprising. As a condition for isomorphous miscibility, Vegard's rule [19] allows deviations in different radii only up to 15%. In the present case the deviation is 20%. This fact accounts

well for a high stabilization potential of the delafossite structure.

Composition dependences of the unit cell volume and lattice constants are given in Table 1 and displayed in Fig. 2. For *x* = 0 (pure CuCrO₂) our *a* and *c* parameter values are in very good agreement with most of those previously reported for powders as well as for single crystal (e.g. *a* = 2.9741(1) Å, *c* = 17.110(2) Å from [20,21]).

The decrease of the unit cell volume with increasing *x* well agrees with the decrease of the ionic radius as chromium (*r* = 0.63 Å) is substituted for aluminum (*r* = 0.51 Å). However, the change is rather anisotropic as it is mainly due to the shrinking of the *a* parameter whereas the *c* parameter remains more or less constant.

Since the Cu–O distance does not vary much in delafossite, this tendency reflects a flattening of the MO₆ octahedra. A nice geometric account of this evolution is given in [22] where the authors suggest that the strong repulsion between M³⁺ ions across the octahedron shared edges reduces the O–O distance to the contact distance.

Therefore the increase of the size of M cation leads to an increase of the octahedron distortion and in turn of the M–M distance that corresponds to the *a* parameter. We may recall that in CuMO₂, as M changes from Al³⁺ to La³⁺, the *a* parameter undergoes a huge increase from 2.8 up to 3.8 Å.

The geometries and electronic structures of CuAl_{1-x}Cr_xO₂ have been investigated using density-functional theory with on-site corrections for strongly correlated systems (GGA+*U*) for *x* = 0, 1/2, 1 [18]. Al is found to be well described within the ionic model, with a valence charge corresponding to a +3 oxidation state. Substituting Cr for Al is predicted to decrease the density of states at the top of the valence band. Analysis of atom-projected densities of states and valence charges suggests that this is due to increased covalency between Cr and O; the valence charge for O in the Cu–O–(Al,Cr) subunits changes from –1.74 to –1.25 when Cr replaces Al. This produces an indirect oxygen mediated change to the Cu *d* states.

Strain generated by the Al substitution was determined from the Williamson-Hall relationship. Plots of (*L*·cosθ) as a function of (sinθ) are given in Fig. 3. They show a remarkable difference in angular dependence of the line width for different families of inter reticular planes: the *h*0*l* planes yield an important contribution of microstrains (high slope), while this effect is almost negligible in 00*l* planes. This shows that this material behaves rather anisotropically, and that strains affects mostly the bonding in the basal *ab* planes.

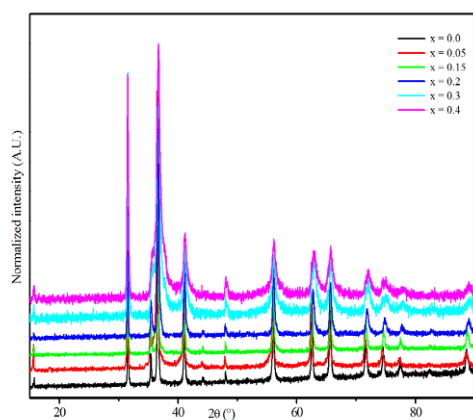


Figure 1. Room temperature XRD patterns of $\text{CuCr}_{1-x}\text{Al}_x\text{O}_2$ ($0 \leq x \leq 0.4$)

Table 1. Cell parameters evolution with Al concentration

	0	0.15	0.2	0.3	0.4
a(Å)	2.9742(1)	2.9699(3)	2.9603(6)	2.9579(7)	2.9573(7)
c(Å)	17.1000(4)	17.0888(5)	17.0711(6)	17.0591(6)	17.0569(8)

Finally note that the oxygen stoichiometry cannot be reliably obtained by X-ray diffraction data, and the presence of three different mixed-valences precludes a reliable use of chemical redox titration. However, all the samples were prepared under the same conditions (initial oxygen stoichiometry, amount of powder) and their oxygen contents are assumed to close to 2 in all cases. This assumption is supported by a previous study of CuCrO_2 showing that this compound does not accommodate large oxygen off-stoichiometry [23]. This could be confirmed by neutron diffraction, which was not available to us during this study.

4. Magnetic properties

We performed the zero-field cooling (ZFC) measurements under 0.1 T magnetic field and the data are shown in Fig. 4.

It can be clearly seen that all the samples are in the paramagnetic states in the temperature range 150–300 K. The magnetization of the samples decreases with increasing Al concentration. For $x = 0.00$, an anomaly appears at 25 K owing to an antiferromagnetic (AFM) transition. The Néel temperature (T_N) is almost consistent with the one previously reported [24]. For $x = 0.05, 0.1$ and 0.15 , the $M-T$ curves exhibit similar shapes when the temperature is greater than 30 K. Anomaly around 120 K for $0 < x < 0.2$ is perhaps due to a very small amount ($< 0.01\%$) of magnetic impurity CuCr_2O_4 . However, the AFM transition does not appear

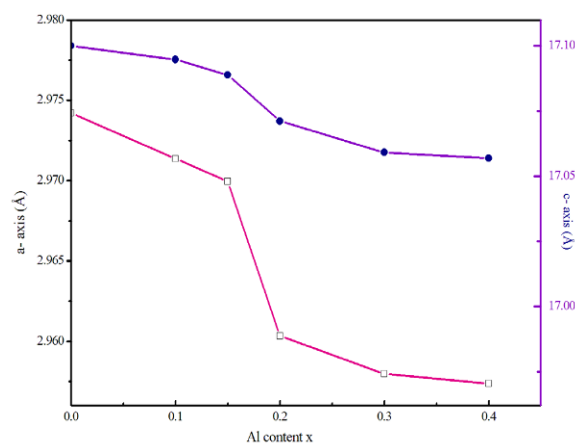


Figure 2. Lattice constants evolution with the Al content

in the whole temperature range for $x = 0.050$ to 0.15 . But then a tiny anomaly in the $M-T$ curves can be seen at about 30 K, which is due to the AFM interaction. For $x \geq 0.2$ no abrupt increase of the magnetization was observed. Samples exhibit a weak paramagnetism varying slightly with temperature.

The structure calculation in [18], shows that, Cr adopts a formal oxidation state of Cr(III) producing a $3d^3$ ion. The approximately octahedral crystal field removes the d orbital degeneracy and increases the energy of the e_g states. The favored electronic configuration is thus high spin t_{2g}^3 . Due to the t_{2g}^3 configuration, AFM interactions are stabilized, while FM interactions result in no net energy gain. The calculated energy difference between the AFM and FM configurations is small at 20 meV/f.u.

Plots of the inverse molar susceptibility $1/\chi$ as a function of the temperature for the $\text{CuCr}_{1-x}\text{Al}_x\text{O}_2$ ($0 \leq x \leq 0.40$) samples are shown in Fig. 5. The plot of $1/\chi$ versus T shows an exactly linear relationship at high temperature, which is well fitted by the Curie–Weiss equation, $\chi = C/(T + \Theta)$ [25]. It indicates that all the $\text{CuCr}_{1-x}\text{Al}_x\text{O}_2$ ($0 \leq x \leq 0.40$) samples are in paramagnetic state at high temperature, while the curves show some nonlinear behavior, which can be attributed to AFM or FM interaction at a low temperature.

The relationship between x and the Curie–Weiss temperature (Θ) can be obtained by fitting the Curie–Weiss equation, and is shown in Fig. 6.

Contrary to some other delafossites such as CuFeO_2 , the magnetic behavior of CuCrO_2 does not clearly reflect the 2D character of the structure [24]. A reason could be the small value of the exchange integral [26] giving only a very small deviation from the Curie–Weiss law above the Néel temperature (25 K). The magnetic behavior of the triangular lattice of the M atoms is dominated by two effects: one is the value

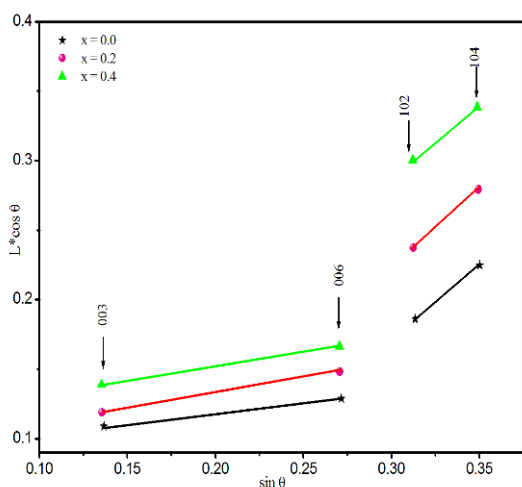


Figure 3. Williamson-Hall plot of integral line width L for different Al concentration

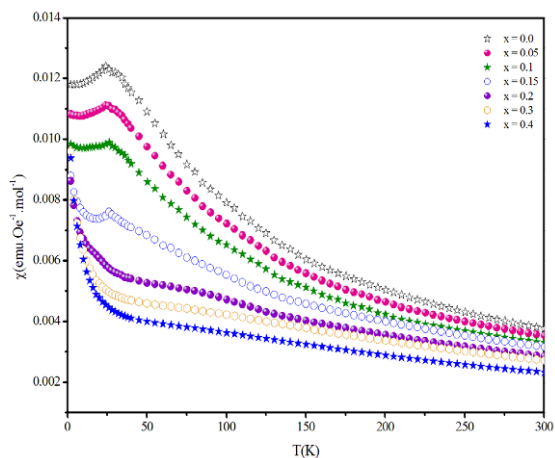


Figure 4. Temperature (T) dependence of zero-field-cooling susceptibility of $\text{CuCr}_{1-x}\text{Al}_x\text{O}_2$ for $0 \leq x \leq 0.4$

of the M–O–M angle close to 95° suggesting a weak or even vanishing superexchange contribution and the other is the frustration. As x increases in $\text{CuCr}_{1-x}\text{Al}_x\text{O}_2$, in addition to the above effects, the number of magnetic nearest neighbors decreases and the onset of magnetic ordering is no longer seen in the plot of the reciprocal magnetic susceptibility versus temperature for $x \geq 0.20$.

Fig. 7 shows the temperature dependence of specific heat (C) for CuCrO_2 ($x = 0$) and $\text{CuCr}_{0.85}\text{Al}_{0.15}\text{O}_2$ ($x = 0.15$).

For both compounds, the electric contribution to specific heat is negligible at low temperatures [17], so the low-temperature specific heat is composed of a lattice contribution (C_{latt}) and a magnetic contribution (C_{mag}); $C = C_{\text{latt}} + C_{\text{mag}}$. To deduce C_{mag} , C_{latt} must be first estimated.

In this paper, the base line of the C - T curve is estimated by a combination of Debye and Einstein models (CD and CE) [27], as expressed by the solid

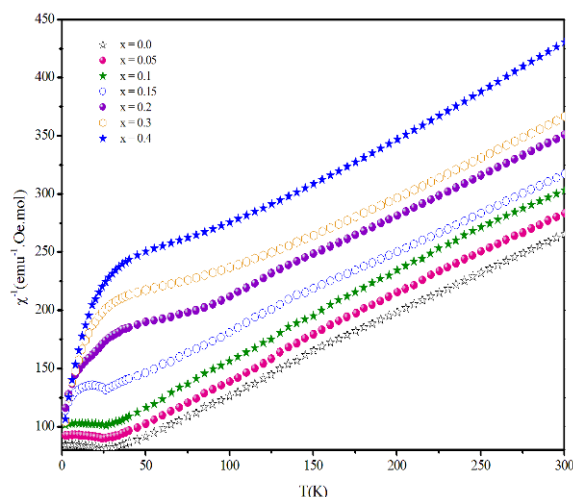


Figure 5. Temperature (T) dependence of the inverse susceptibility of $\text{CuCr}_{1-x}\text{Al}_x\text{O}_2$ for $0 \leq x \leq 0.4$

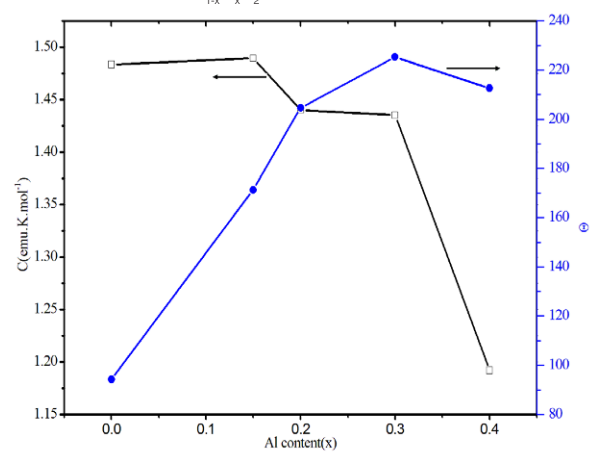


Figure 6. The variation of the Curie-Weiss parameters with the Al concentration x .

lines in Figs. 7a and 7b. The T dependence of C_{mag}/T for CuCrO_2 and $\text{CuCr}_{0.85}\text{Al}_{0.15}\text{O}_2$ are shown in Fig. 8. This figure clearly shows that the specific heat peak at T_N becomes broader and that the peak temperature (T_{peak}) decreases as x increases. Such x dependence of C is apparently correlated with that of magnetization (M) [28].

Corresponding to the AFM transition, a sharp peak is observed at about 25 K. In addition to the sharp peak, a broad shoulder is observed around 25 K. Such a broad C_{mag} (T) peak profile is often observed in frustrated kagome [29] or triangular [30] AFM lattices, and indicates high degeneracy due to magnetic frustration. Neutron diffraction measurements have shown that CuCrO_2 gives rise to a 120° spin structure [31], so the C_{mag} (T) profiles may be due to residual magnetic frustration stemming from deviation from a complete 120° spin structure. Such shoulders in C_{mag} (T) around 25 K were also observed for all $\text{CuCr}_{1-x}\text{Mg}_x\text{O}_2$ compounds [32].

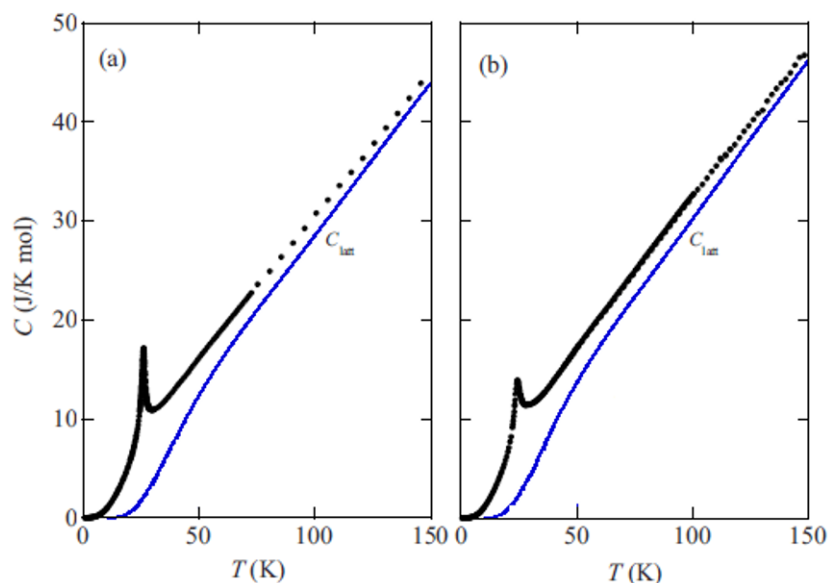


Figure 7. Temperature dependence of specific heat (C) of $\text{CuCr}_{1-x}\text{Al}_x\text{O}_2$ for: $x = 0$ (a) and $x = 0.15$ (b).

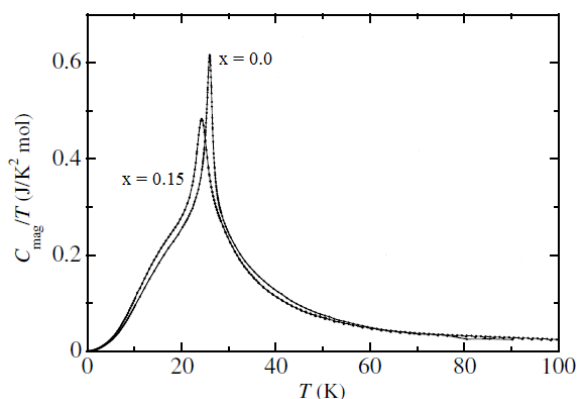


Figure 8. x dependence of C_{mag}/T vs T for $\text{CuCr}_{1-x}\text{Al}_x\text{O}_2$.

5. Conclusion

Introducing Al into the Cr lattice sites in alternating ab layers has a significant effect on the structure. The occupied Cr $3d$ states interact covalently with the neighboring O atoms and hence indirectly modify the

Cu $3d$ states, an effect that the $2p6$ Al atoms are unable to produce. This decreases the density of states at the top of the valence band, which are precisely the states expected to determine the mobility of p -type charge carriers formed on doping. Temperature dependence of the magnetic susceptibility shows that a long range order takes place at low temperature for $x \leq 0.2$. For higher dilution rates of magnetic ions ($x \geq 0.20$) the temperature dependence of the magnetic susceptibility no longer accounts for long range ordering at least above 4 K.

Acknowledgements

This work was financially supported by Université Joseph Fourier (UJF-Chimie), Grenoble, France.

References

- [1] R.D. Shannon, D.B. Rogers, C.T. Prewitt, *Inorg. Chem.* 10, 713 (1971)
- [2] J.P. Doumerc, A. Ammar, A. Wichainchai, M. Pouchard, P. Hagenmuller, *J. Phys. Chem. Solids* 48, 37 (1987)
- [3] H. Kawazoe, M. Yasukawa, H. Hyodo, M. Kurita, H. Yanagi, H. Hosono, *Nature* 389, 939 (1997)
- [4] J.R. Monnier, G.R. Apai, M.J. Hanrahan, U.S. Patent 4748144-A (1988)
- [5] K. El Ataoui, J.P. Doumerc, A. Ammar, J.C. Grenier, L. Fournes, A. Wattiaux, M. Pouchard, *Solid State Sci.* 7, 710 (2005)
- [6] H. Yagi, W. Seo, K. Koumoto, *Key Eng. Mater.* 251, 180 (2000)
- [7] K. Isawa, Y. Yaegashi, S. Ogota, M. Nagano, S. Sudo, K. Yamada, H. Yamauchi, *Phys. Rev. B* 57, 7950 (1998)
- [8] R.D. Shannon, *Acta Crystallogr., Sect. A* 32, 751

- (1976)
- [9] M. Hasegawa, M.I. Batrashevich, T.R. Zhao, H. Takei, T. Goto, *Phys. Rev. B* 63, 184437 (2001)
- [10] S. Mitsuda, Y. Matsumoto, T. Wada, K. Kurihara, Y. Urata, H. Yoshizawa, M. Mekata, *Physica B* 213–214, 194 (1995)
- [11] Y. Ajiro, K. Hanasaki, T. Asano, T. Takagi, M. Mekata, H. Aruga Katori, T. Goto, *J. Phys. Soc. Jpn.* 64 3643 (1995)
- [12] Y. Oohara, M. Mekata, T. Morishita, K. Kakurai, M. Nishi, T.R. Zhao, H. Takei, *J. Phys. Soc. Jpn.* 70, 3031 (2001)
- [13] N. Terada, S. Mitsuda, S. Suzuki, M. Fukuda, T. Kawasaki, T. Nagao, H. Aruga Katori, *J. Phys. Soc. Jpn.* 73, 1442 (2004)
- [14] N. Terada, S. Mitsuda, K. Prokes, O. Suzuki, H. Kitazawa, H.A. Katori: *Phys. Rev. B* 70, 174412 (2004)
- [15] N. Terada, S. Mitsuda, Y. Oohara, H. Yoshizawa, H. Takei, *J. Magn. Magn. Mater.* 272–276, E997 (2004) Suppl. 1
- [16] N. Terada, T. Kawasaki, S. Mitsuda, H. Kimura, Y. Noda, *J. Phys. Soc. Jpn.* 74, 1561 (2005)
- [17] T. Okuda, Y. Beppu, Y. Fujii, T. Onoe, N. Terada, S. Miyasaka, *Phys. Rev. B* 77, 134423 (2008)
- [18] D.O. Scanlon, A. Walsh, B.J. Morgan, G.W. Watson *Phys. Rev. B* 79, 035101 (2009)
- [19] L. Vegard, H. Schielderup, *Phys. Z.* 18, 93 (1917)
- [20] R.D. Shannon, D.B. Rogers, C.T. Prewitt, *Inorg. Chem.* 10, 713 (1971)
- [21] C.T. Prewitt, R.D. Shannon, D.B. Rogers, *Inorg. Chem.* 10, 719 (1971)
- [22] J. Tate, M.K. Jayaraj, A.D. Draeseke, T. Ulbrich, A.W. Sleight, K.A. Vanaja, R. Nagarajan, J.F. Wagner, R.L. Hoffman, *Thin Solid Films* 411, 119 (2002)
- [23] L. Da, F. Xiaodong, D. Weiwei, D. Zanhong, T. Ruhua, Z. Shu, J. Wang, T. Wang, Y. Zhao, X. Zhu *J. Phys. D: Appl. Phys.* 42, 055009 (2009)
- [24] H. Kadoeaki, H. Kikuchi, Y. Ajiro, *J. Phys.: Condens. Matter* 2, 4485 (1990)
- [25] T. Okuda, N. Jufuku, S. Hidaka, N. Terada, *Phys. Rev. B* 72, 144403 (2005)
- [26] N. Terada, S. Mitsuda, T. Fujii, K. Soejima, I. Doi, H.A. Katori, Y. Noda, *JPSJ* 74, 2604 (2005)
- [27] E.S.R. Gopal, *Specific Heats at Low Temperatures* (Plenum, New York, 1966)
- [28] T. Okuda, N. Jufuku, S. Hidaka, N. Terada, *Phys. Rev. B* 72, 144403 (2005)
- [29] A.P. Ramirez, B. Hessen, M. Winklemann, *Phys. Rev. Lett.* 84, 2957 (2000)
- [30] S. Nakatsuji, Y. Nambu, H. Tonomura, O. Sakai, S. Jonas, C. Broholm, H. Tsunetsugu, Y. Qiu, Y. Maeno, *Science* 309, 1697 (2005)
- [31] (a) H. Kadowaki, H. Kikuchi, Y. Ajiro, *J. Phys.: Condens. Matter* 2, 4485 (1990); (b) Y. Oohara, S. Mitsuda, H. Yoshizawa, N. Yaguchi, H. Kuriyama, T. Asano, M. Mekata, *J. Phys. Soc. Jpn.* 63, 847 (1994)
- [32] T. Okuda, Y. Beppu, Y. Fujii, T. Kishimoto, K. Uto, T. Onoe, N. Jufuku, S. Hidaka, N. Terada, S. Miyasaka, *Journal of Physics: Conference Series* 150, 042157 (2009)